Article

A Transport Corrected SP_3 Solver Based on Nodal Expansion Formulation for Equivalent Core Calculations

Yuchao Xu [1], Jason Hou [1,*] and Kostadin Ivanov [1]

[1] Department of Nuclear Engineering, North Carolina State University, Raleigh, NC 27695
* Correspondence: jason.hou@ncsu.edu

Abstract: The Simplified Spherical Harmonic (SP_N) approximation was first introduced as a three-dimensional (3-D) extension of the plane-geometry Spherical Harmonic (P_N) equations. A third order SP_N (SP_3) solver, recently implemented in the Nodal Expansion Method (NEM), has shown promising performance in the reactor core neutronics simulations. This work is focused on the development and implementation of the transport corrected interface and boundary conditions in NEM SP_3 solver, following recent published work on the rigorous SP_N theory for piecewise homogeneous regions. A streamlined procedure has been developed to generate the flux zero and second order/moment discontinuity factors (DFs) of the generalized equivalence theory to eliminate the error introduced by pin-wise homogenization. Moreover, several color set models with varying size and configuration are later explored for their capability of generating DFs that can produce results equivalent to that using the whole-core homogenization model for more practical implementations. The new developments are tested and demonstrated on the C5G7 benchmark. The results show that the transport corrected SP_3 solver shows general improvements to power distribution prediction compared to the basic SP_3 solver with no DFs or only zero order/moment DFs. The complete equivalent calculations using the DFs can almost reproduce transport solutions with high accuracy. The use of equivalent parameters from larger size color set models show better prediction in the whole-core calculations. By coupling different color set models DFs can offer the best accuracy at both eigenvalues and power distributions.

Keywords: Transport Corrected SP_3, Nodal Expansion Method, Generalized Equivalence Theory, Discontinuity Factors

1. Introduction

Obtaining solutions to the neutron transport equation with consistent angular discretization, such as discrete ordinates (S_N) or spherical harmonics (P_N), for the 3-dimentaional (3-D) transport problem can be challenging, even with the rapid increase of computing power. Thus, low-order approximations to the transport equation that can be solved at a significantly reduced computational cost are of special interest. The coarse mesh diffusion equations are traditionally the first choice to the program developer; however, such methods may be inadequate for advanced reactor designs, which usually demonstrate high level of heterogeneity, or in core regions near material boundaries and strong absorbers.

The Simplified P_N (SP_N) equations were first proposed to introduce additional transport effects into the standard P_1 equations without introducing the complexities and undesired increase in the computational cost that a full transport theory solution would entail. The P_N equations are obtained from inserting the truncated spherical harmonics expansion (to some order n) of the angular flux and differential scattering cross section into the transport equation.

By replacing the derivatives of the one-dimensional (1-D) P_N equation in planar geometry with the 3-D gradient and divergence operators, one arrives at 3-D generalization of the 1-D P_N equations [1]. Such substitution was performed in an *ad hoc* manner, leaving

the method to lack of theoretical foundation. As asymptotic and variational derivations later assisted to establish the theoretical basis for the SP_N method [2-4], the application of the method became more popular. The numerical results show that the SP_N approximation can yield accurate solutions of the transport problems, which outperforms diffusion method, but with considerably less computational expense than those for the S_N or the full P_N methods [5,6]. For example, the computational time for SP_3 is only about twice as that of the diffusion method. At locations in the core with high flux gradient, such as material boundaries, the SP_3 has a higher precision due to the use of the higher legendary moments P_N scattering library and angular flux distribution. It is suggested that the SP_3 method should be utilized to a homogenized pin cell (other than a large assembly node) level calculation using a few groups (instead of 2 groups) to retain its superiority in accuracy over diffusion approximation [7].

The NEM (Nodal Expansion Method) code has been developed for 3-D whole-core steady state and transient analysis with cartesian, hexagonal, and cylindrical geometries. A SP_3 solver was established in NEM by taking advantage of the original diffusion-based solver to achieve a pin cell resolution of highly heterogeneous reactor cores [8]. Further development and enhancement have since been conducted to improve its performance, such as incorporating the higher order scattering cross sections and discontinuity factors (DFs) [9,10]. However, this implementation adopted the *ad hoc* interface and boundary conditions based on the assumption of 1-D behavior near a surface, which presents the angular flux from being represented by the SP_N flux components. Therefore, SP_N solver cannot provide the exact scalar flux solution as by the P_N solver.

This work is focused on the development and implementation of the interface and boundary conditions in NEM SP_3 solver, following recent published work on the rigorous SP_N theory for piecewise homogeneous regions [11,12]. The new theory proves that the SP_N solutions can represent a particular set of the angular flux solution by the P_N theory. The resulting interface and boundary conditions now involve terms of higher order gradients of flux as well as tangential gradients, although the SP_N equations are identical to the conventional ones. The transported corrected interface and boundary conditions are formulated in the nodal expansion expression of the flux components and the solution method involving the response matrix utilized in NEM. Then, a side-dependent DF generation approach is devised based on the generalized equivalence theory (GET) for homogenization with the intention to eliminate the error introduced by pin-wise homogenization. Both zeroth- and second-moment DFs can be generated using an in-house developed code using the solution from the transport solutions using Method of Characteristics (MOC). Several color set models with varying size and configuration are later explored for their capability of generating DFs that can produce results equivalent to that using the whole-core model for more practical implementations. The new developments are tested and demonstrated on the C5G7 benchmark.

This paper is organized in the following. In Section 2, the SP_3 equations based on the nodal expansion formulation are derived and the solution method of SP_3 equations using the response matrix is introduced. Section 3 is focused on the derivation of the interface and boundary conditions in the new SP_N theory and their implementation in the NEM SP_3 solver. Section 4 introduces the equivalent calculation scheme developed for the SP_3 solver with the emphasis placed on the generation of equivalence parameters using different lattice models to facilitate practical applications. The transport corrected SP3 solver is tested on a series of problems from the C5G7 benchmark, and the results are shown in Section 5. Finally, conclusions and future perspectives are given in Section 6.

2. SP_3 Method based on Nodal Expansion Formulation

For the general case with odd n, the SP_N equations can reduce to (n+1)-th order differential equation for the lowest order scalar flux, which is equivalent to $(n+1)/2$ coupled second order differential equations. This indicates that being diffusion theory type equations, the SP_N solvers have commonly been cast in such a way as to leverage existing

diffusion machinery by iterating over the SP_N moment equations. The steady-state SP_3 equations used in NEM are the following [8]:

$$\begin{aligned} -D_{0,g}\nabla^2\Phi_{0,g}(r) + \Sigma_{r,0,g}\Phi_{0,g}(r) - 2\Sigma_{r,0,g}\phi_{2,g}(r) &= S_{0,g}(r) \\ -D_{2,g}\nabla^2\phi_{2,g}(r) + \left[\Sigma_{r,2,g} + \frac{4}{5}\Sigma_{r,0,g}\right]\phi_{2,g}(r) - \frac{2}{5}\Sigma_{r,0,g}\Phi_{0,g}(r) &= -\frac{2}{5}S_{0,g}(r), \end{aligned} \tag{1}$$

where the unknowns are the synthesized *zero*-th moment flux approximation $\Phi_0 = \phi_0 + 2\phi_2$ and the second moment flux ϕ_2 in all energy groups, Σ_r is the transport corrected removal macroscopic cross section, and the source terms on the right-hand side of the equations $S_{0,g}$ is the sum of the scattering and fission source associated with the *zero*-th moment flux

$$S_{0,g} = \sum_{g'=1,g'\neq g}^{G} \Sigma_{s,0,g'\to g}\phi_{0,g'} + \frac{\chi_g}{k_{\text{eff}}}\sum_{g'=1}^{G} \Sigma_{f,0,g'}\phi_{0,g'}, \tag{2}$$

where Σ_s and Σ_f are the scattering and fission cross sections, respectively, and χ is the fission spectrum. Note that the scattering matrix $\Sigma_{s,0,g'\to g}$ includes only the isotropic scattering source, while the higher moments are approximated by the transport corrected removal cross section Σ_r. The two diffusion coefficients are defined as $D_0 = 1/3\Sigma_{r,0,g}$ and $D_2 = 9/35\Sigma_{r,2,g}$.

The Marshak boundary conditions in terms of surface fluxes and incoming (j^+) and outward (j^-) partial currents, as used in NEM, are:

$$\begin{aligned} \Phi_0 &= \frac{56}{25}(j_1^+ + j_1^-) + \frac{24}{15}(j_3^+ + j_3^-) \\ \Phi_0 &= \frac{8}{25}(j_1^+ + j_1^-) + \frac{32}{15}(j_3^+ + j_3^-) \end{aligned} \tag{3}$$

In NEM, the 3D gradient operator is splitted to three directions, i.e. $\nabla^2 = \frac{\partial^2}{\partial x^2} + \frac{\partial^2}{\partial y^2} + \frac{\partial^2}{\partial z^2}$ and the same equations are used in all directions. In an arbitrary node with constant neutronic properties and dimensions Δx, Δy, and Δz in the Cartesian geometry, apply the transverse integration approximation, where Eq. (1) is spatially integrated over the two dimensions transverse to the particular direction of interst. The resulting equations in the x direction takes the form

$$\begin{aligned} -D_{0,g}\frac{d^2}{dx^2}\Phi_{0,g}(x) + \Sigma_{r,0,g}\Phi_{0,g}(x) - 2\Sigma_{r,0,g}\phi_{2,g}(x) &= S_{0,g}(x) + L_{y,1,g}(x) + L_{z,1,g}(x) \\ -D_{2,g}\frac{d^2}{dx^2}\phi_{2,g}(x) + \left[\Sigma_{r,2,g} + \frac{4}{5}\Sigma_{r,0,g}\right]\phi_{2,g}(x) - \frac{2}{5}\Sigma_{r,0,g}\Phi_{0,g}(x) &= -\frac{2}{5}S_{0,g}(x) + L_{y,3,g}(x) + L_{z,3,g}(x), \end{aligned} \tag{4}$$

where the transverse integrated *zero*-th and second moment flux are

$$\begin{aligned} \Phi_{0,g}(x) &= \frac{1}{\Delta y \Delta z}\int_{-\Delta y/2}^{\Delta y/2}\int_{-\Delta z/2}^{\Delta z/2} \Phi_{0,g}(x,y,z)\,dzdy \\ \phi_{2,g}(x) &= \frac{1}{\Delta y \Delta z}\int_{-\Delta y/2}^{\Delta y/2}\int_{-\Delta z/2}^{\Delta z/2} \phi_{2,g}(x,y,z)\,dzdy \end{aligned} \tag{5}$$

and first moment transverse leakage term

$$L_{y,1,g}(x) = D_{0,g}\frac{1}{\Delta y \Delta z}\int_{-\Delta y/2}^{\Delta y/2}\int_{-\Delta z/2}^{\Delta z/2} \frac{\partial^2}{\partial y^2}\Phi_{0,g}(x,y,z)\,dzdy \tag{6}$$

$$L_{z,1,g}(x) = D_{0,g}\frac{1}{\Delta y \Delta z}\int_{-\Delta y/2}^{\Delta y/2}\int_{-\Delta z/2}^{\Delta z/2}\frac{\partial^2}{\partial z^2}\Phi_{0,g}(x,y,z)\,dzdy.$$

and the transverse integrated source term

$$S_{0,g}(x) = \frac{1}{\Delta y \Delta z}\int_{-\Delta y/2}^{\Delta y/2}\int_{-\Delta z/2}^{\Delta z/2} S_{0,g}(x,y,z)\,dzdy. \tag{7}$$

Replacing Φ_0 by ϕ_2 in Eq. (5) yields the third moment trasverse leakage terms $L_{y,3,g}(x)$ and $L_{z,3,g}(x)$.

In the context of the NEM, the intra-node flux moments $\Phi_0(x)$ and $\phi_2(x)$ are is expanded in series within each node using fourth-order polynomial basis functions as follows:

$$\begin{aligned}\Phi_0(x) &= \bar{\Phi}_0 + \Sigma_{n=1}^4 a_n f_n \\ \phi_2(x) &= \bar{\phi}_2 + \Sigma_{n=1}^4 b_n f_n,\end{aligned} \tag{8}$$

where $\bar{\Phi}_0$ and $\bar{\phi}_2$ are the node average flux moments and the polinomials are

$$\begin{aligned} f_1 &= \frac{x}{\Delta x} \\ f_2 &= 3\left(\frac{x}{\Delta x}\right)^2 - \frac{1}{4} \\ f_3 &= \left(\frac{x}{\Delta x}\right)^3 - \frac{1}{4}\left(\frac{x}{\Delta x}\right) \\ f_4 &= \left(\frac{x}{\Delta x}\right)^4 - \frac{3}{10}\left(\frac{x}{\Delta x}\right)^2 + \frac{1}{8}\end{aligned}. \tag{9}$$

Here we drop the energy group index g and focus on the mono-energetic expression for simplicity.

The expansion coefficients a and b can be determined by solving Eq. (3) at specific locations, i.e., left node edge $x = -\Delta x/2$ and right node edge $x = \Delta x/2$. Introducing the node edge flux moments, including $\Phi_{0,L}$ and $\phi_{2,L}$ on the left edge, and $\Phi_{0,R}$ and $\phi_{2,R}$ on the right edge yields

$$\begin{aligned} a_1 &= \Phi_{0,R} - \Phi_{0,L} \\ a_2 &= \Phi_{0,R} + \Phi_{0,L} - 2\bar{\Phi}_0 \\ b_1 &= \phi_{2,R} - \phi_{2,L} \\ a_2 &= \phi_{2,R} + \phi_{2,L} - 2\bar{\phi}_2. \end{aligned} \tag{10}$$

Next, multiply f_1 and f_2 to Eq. (3), perform the transverse integration $\frac{1}{\Delta x}\int_{-\Delta x/2}^{\Delta x/2} dx$, define flux-like terms

$$\begin{aligned} \overline{\Phi}_{0,x,1} &= \langle f_1, \Phi_0(x)\rangle = \frac{1}{\Delta x}\int_{-\Delta x/2}^{\Delta x/2} f_1 \Phi_0 dx \\ \overline{\Phi}_{0,x,2} &= \langle f_2, \Phi_0(x)\rangle = \frac{1}{\Delta x}\int_{-\Delta x/2}^{\Delta x/2} f_2 \Phi_0 dx \\ \overline{\phi}_{2,x,1} &= \langle f_1, \phi_2(x)\rangle = \frac{1}{\Delta x}\int_{-\Delta x/2}^{\Delta x/2} f_1 \phi_2 dx \\ \overline{\phi}_{2,x,2} &= \langle f_2, \phi_2(x)\rangle = \frac{1}{\Delta x}\int_{-\Delta x/2}^{\Delta x/2} f_2 \phi_2 dx \end{aligned} \tag{11}$$

and the rest expansion coefficient can be derived as

$$\begin{aligned} a_3 &= 10a_1 - 120\overline{\Phi}_{0,x,1} \\ a_4 &= 35a_2 - 700\overline{\Phi}_{0,x,2} \\ b_3 &= 10b_1 - 120\overline{\phi}_{2,x,1} \\ b_4 &= 5b_2 - 700\overline{\phi}_{2,x,2} \end{aligned}. \tag{12}$$

Note that the expression of the flux-like terms can be derived from the 1-D SP_3 equations shown in Eq. (4) by multiply f_1 and f_2, and then performing the transverse integration along one direction

$$\begin{aligned} \overline{\Phi}_{0,x,1} &= -\frac{1}{\Sigma_{r,0}}\left[\frac{1}{2\Delta x}\left(J_{1,x,R}+J_{1,x,L}\right)+\frac{D_0}{\Delta x^2}\left(\Phi_{0,R}-\Phi_{0,L}\right)-2\Sigma_{r,0}\overline{\phi}_{2,x,1}\right. \\ &\qquad \left. -S_{0,x,1}+\frac{1}{\Delta y}L_{y,1,1}+\frac{1}{\Delta z}L_{z,1,1}\right] \\ \overline{\Phi}_{0,x,2} &= -\frac{1}{\Sigma_{r,0}}\left[\frac{1}{2\Delta x}\left(J_{1,x,R}-J_{1,x,L}\right)+3\frac{D_0}{\Delta x^2}\left(\Phi_{0,R}+\Phi_{0,L}\right)-2\Sigma_{r,0}\overline{\phi}_{2,x,2}\right. \\ &\qquad \left. -S_{0,x,2}+\frac{1}{\Delta y}L_{y,1,2}+\frac{1}{\Delta z}L_{z,1,2}-\frac{6D_0}{\Delta x^2}\overline{\Phi}_0\right] \\ \overline{\phi}_{2,x,1} &= -\frac{1}{\alpha}\left[\frac{1}{2\Delta x}\left(J_{3,x,R}+J_{3,x,L}\right)+\frac{D_2}{\Delta x^2}\left(\phi_{2,R}-\phi_{2,L}\right)-\frac{2}{5}\Sigma_{r,0}\overline{\Phi}_{0,x,1}\right. \\ &\qquad \left. +\frac{2}{5}S_{0,x,1}+\frac{1}{\Delta y}L_{y,3,1}+\frac{1}{\Delta z}L_{z,3,1}\right] \\ \overline{\phi}_{2,x,2} &= -\frac{1}{\alpha}\left[\frac{1}{2\Delta x}\left(J_{3,x,R}-J_{3,x,L}\right)+\frac{3D_2}{\Delta x^2}\left(\phi_{2,R}+\phi_{2,L}\right)-\frac{2}{5}\Sigma_{r,0}\overline{\Phi}_{0,x,2}\right. \\ &\qquad \left. +\frac{2}{5}S_{0,x,2}+\frac{1}{\Delta y}L_{y,3,2}+\frac{1}{\Delta z}L_{z,3,2}-\frac{6D_2}{\Delta x^2}\bar{\phi}_2\right] \end{aligned}, \tag{13}$$

where $\alpha = \Sigma_{r,2}+\frac{4}{5}\Sigma_{r,0}$, the $J_{n,x,L}$ and $J_{n,x,R}$ are the node edge net currents on the left (L) and right (R) edge, respectively.

In the above, $L_{i,n,k} = \frac{1}{\Delta x}\int_{-\Delta x/2}^{\Delta x/2} L_{i,n} f_k dx$ is the transverse integrated transverse leakage term, where i refers to the direction (y or z), n is the flux moments (1 or 3), and k is the index integration function or polynomial (1 or 2). The new source term $S_{0,k} = \frac{1}{\Delta x}\int_{-\Delta x/2}^{\Delta x/2} S_0 f_k dx$ is obtained in the same way.

In calculation mechanism in NEM requires all quantities of interest to be derived in terms of the partial currents and formulated in the response matrix, which expresses the outgoing partial currents as a function of incoming partial currents and intra-node as well as sources and sinks. The response matrix is derived from Fick's Law for the partial currents on the node boundaries, using the x-axis as an example,

$$\begin{aligned} J_{1,x,L} &= j_1^+\left(-\frac{\Delta x}{2}\right)-j_1^-\left(-\frac{\Delta x}{2}\right) = D_0\frac{d}{dx}\Phi_0(x)\Big|_{-\Delta x/2} \\ J_{1,x,R} &= j_1^+\left(\frac{\Delta x}{2}\right)-j_1^-\left(\frac{\Delta x}{2}\right) = -D_0\frac{d}{dx}\Phi_0(x)\Big|_{\Delta x/2} \\ J_{3,x,L} &= j_3^+\left(-\frac{\Delta x}{2}\right)-j_3^-\left(-\frac{\Delta x}{2}\right) = D_2\frac{d}{dx}\phi_2(x)\Big|_{-\Delta x/2} \\ J_{3,x,R} &= j_3^+\left(\frac{\Delta x}{2}\right)-j_3^-\left(\frac{\Delta x}{2}\right) = -D_2\frac{d}{dx}\phi_2(x)\Big|_{-\Delta x/2}, \end{aligned} \tag{14}$$

where j_1^+ and j_1^- are the outgoing and incoming partial currents, respectively. Substituting the polynomial expansion in Eq. (3) to the equation above and performing differentiation yields four equations in each of three directions. Take the right edge of the node $x = \Delta x/2$ for example, the partial currents are

$$\begin{aligned} j_{1,R}^+ &= j_{1,R}^- + \frac{1}{\Delta x}\left(a_1+3a_2+\frac{a_3}{2}+\frac{a_4}{5}\right) \\ j_{3,R}^+ &= j_{3,R}^- + \frac{1}{\Delta x}\left(b_1+3b_2+\frac{b_3}{2}+\frac{b_4}{5}\right). \end{aligned} \tag{15}$$

while similar expressions can be obtained for $j_{1,L}^+$ and $j_{3,L}^+$.

Recall that the expansion coefficients $a_1 - a_4$ and $b_1 - b_4$ are functions of the node-average flux, node edge fluxes, and flux-like terms, as shown in Eq. (4-7), which can be expressed in terms of the partial currents. The node-average flux $\bar{\Phi}_0$ and $\overline{\phi}_0$ required in Eq. (4) can be obtained by integrating the neutron balance equation (Eq. (2)) over the node volume. Substitution for the node-average flux and flux-like terms (Eq. (7)) in Eq. (9) yields the 4 partial current equations in the x-direction. This derivation is straight-forward but the algebra is quite involved, and thus not shown in detail here. More information can be found in [13]. Note that all 12 partial current equations in the 3 directions are coupled on the right-hand side through the leakage transverse leakage and source terms. Rewriting them in the matrix form we arrive at the response matrix equation

$$\mathbb{A} \cdot \mathbb{J}^+ = \mathbb{C} \cdot \mathbb{J}^- + \mathbb{B}_1 \cdot \mathbb{S} + \mathbb{B}_2 \cdot \mathbb{L}. \tag{16}$$

where in principle $\mathbb{J}^+$, $\mathbb{J}^-$, $\mathbb{S}$, and $\mathbb{L}$ are 12×1 vectors, and the coefficient matrices are with the size of 12×12, although the actual implementation differs slightly from this representation [13].

The eigenvalue problem is solved by NEM using the traditional inner/outer iteration method. For each group, inner iterations, or multiple sweeps through the mesh with a known internal source are performed to invert the within-group SP_3 removal matrix. Outgoing partial currents are computed using the incoming partial currents and the node dependent response functions. Theses outgoing partial currents become the incoming partial currents in the neighboring nodes. Outer fission source iterations are then performed around the inner iterations to calculate values for the problem multiplicative eigenvalue (k_{eff}) and the space- and energy-dependent fission neutron source distribution.

3. Transport Corrected SP3 Method for Equivalent Calculations

3.1. Derivations of Interface and Boundary Conditions

Homogenization techniques have been used in nuclear reactor analysis to reduce the spatial and angular domain complexity of a nuclear reactor by replacing pre-calculated heterogeneous subdomains by homogeneous ones and using low order solver to solve the homogeneous problem. To guarantee this equivalence especially for the fission rate and leakage rate in neutron balance equation, two main factors should be guaranteed: 1) homogeneous cross sections are calculated based on the spectrum of neutron fluxes to preserve the fission rate; 2) at node interfaces, first order flux (J_1) should be preserved to make consistent of leakage rate between heterogeneous and homogeneous calculations.

To achieve the second objective, DFs should be generated at the boundaries of the homogenized nodes as defined in GET [14], which was derived from the equivalence theory [15]. However, performing the complete equivalent calculation using the DF for SP_3 has long been problematic due to the *ad hoc* interface and boundary conditions adopted in the early developments of the SP_N theory, which involves the diffusion theory type of first order derivatives in the surface normal direction. It prevents the angular flux from being represented by the SP_3 solution in the conventional SP_3 theory or being compared to the reference angular flux solution the from heterogeneous transport calculation. Simply put, it is not clear which higher order quantities should be continuous across the node surface, which makes it difficult to rigorously define and calculate the high order DF in SP_3.

In a recent work, Chao rederived the SP_N equations from the P_N, proved that ϕ_0 solutions in 3-D SP_3 are one set of solution to 3-D P_3 theory, and provided exact expression of the angular flux using the SP_3 flux solutions [11-12]. This method has been adopted, modified, and implemented in the NEM SP_3 solver. For the convenience of the readers, we provide a concise review summary of Chao's work regarding the derivation of the transport corrected interface and boundary conditions.

The derivation starts by decomposing the transport equation is into an even parity part and an odd parity part:

$$\psi(\Omega, r) = \psi_E(\Omega, r) \pm \psi_O(\Omega, r) \tag{17}$$

$$-\frac{1}{\Sigma_t}(\Omega \cdot \nabla)^2 \psi_E(\Omega, r) + \Sigma_t \psi_E(\Omega, r) = \frac{Q(r)}{4\pi} \tag{18}$$

$$\psi_O(\Omega, r) = -\frac{1}{\Sigma_t}\Omega \cdot \nabla \psi_E(\Omega, r). \tag{19}$$

It was shown that the SPN equations can be derived via the variational method by introducing the following trial function into the even parity transport equation (Eq. (18)):

$$\psi_E(\Omega, r) = \frac{1}{4\pi} \sum_{even\ n} (2n+1)[L_n(\Omega, \nabla)\mathcal{F}_n] \tag{20}$$

The operator $L_n(\Omega, \nabla) = \sum_{2k=0}^{n} a_{n,n-2k}[(\Omega \cdot \nabla)^{n-2k}\nabla^{2k}]$ and the coefficients $a_{n,k}$ are the same as those in Legendre polynomial P_n. The functions $\mathcal{F}_n$ are called auxiliary functions with the property:

$$\phi_n(r) = \nabla^n \mathcal{F}_n(r) \tag{21}$$

Note that substituting Eq. (21) into the SPn equation will yield the expression of the auxiliary function $\mathcal{F}_n$. By defining a dimensionless "unit vector" $\hat{\nabla} = \nabla(\nabla^2)^{-1/2}$, the operator $L_n(\Omega, \nabla)$ can be rewritten in terms of Legendre polynomials:

$$L_n(\Omega, \nabla) = \sum_{2k=0}^{n} a_{n,n-2k}[(\Omega \cdot \nabla)^{n-2k}]\,\nabla^n = P_n(\Omega \cdot \hat{\nabla})\nabla^n. \tag{22}$$

Therefore, the trial function Eq. (19) can be rewritten as

$$\psi_E(\Omega, r) = \sum_{even\ n} \frac{2n+1}{4\pi}\left[P_n(\Omega \cdot \hat{\nabla})\nabla^n\right]\mathcal{F}_n. \tag{23}$$

Eq. (23) is important not only because it can lead to the exact SPn equations (by plugging it into Eq. (18)), but also because it gives the angular flux for the SPn theory because Eq. (23) can be reconstructed in terms of the SPN solution functions, as shown below.

To derive the boundary and interface conditions, use the angular flux on a node surface. The angular partial currents going out or in through a surface with the normal vector $\hat{n}$ are defined as:

$$J_k^{\pm}(r) = \hat{n} \cdot \Omega[\psi_E(\Omega, r) \pm \psi_O(\Omega, r)]. \tag{24}$$

To calculate the *k*-th even order moment of the partial currents, Eq. (22) is multiplied by the *k*-th even order Legendre polynomial of the cosine of the polar angle with respect to the normal vector $\hat{n}$, and is then integrate it over the angular space:

$$j_k^{\pm}(r) = \int_{\hat{n}\cdot\Omega>0} P_k(\hat{n} \cdot \Omega)(\hat{n} \cdot \Omega)\psi_E(\Omega, r)d\Omega \pm \int P_k(\hat{n} \cdot \Omega)(\hat{n} \cdot \Omega)\psi_O(\Omega, r)d\Omega, \tag{25}$$

Replacing the even parity angular flux by Eq. (22) and making use of the relationship in Eq. (19) leads to:

$$j_k^{\pm}(r) = \Psi_k(r) \pm \frac{1}{2}J_k(r) \tag{26}$$

and

$$\Psi_k(r) = \int_{\hat{n}\cdot\Omega>0} P_k(\hat{n} \cdot \Omega)(\hat{n} \cdot \Omega)\left\{\sum_{even\ n} \frac{2n+1}{4\pi}\left[P_n(\Omega \cdot \hat{\nabla})\nabla^n\right]\mathcal{F}_n\right\}d\Omega \tag{27}$$

$$J_k(r) = \int P_k(\hat{n}\cdot\Omega)(\hat{n}\cdot\Omega)\left\{\sum_{odd\ n}\frac{2n+1}{4\pi}\left[P_n(\Omega\cdot\hat{\nabla})\nabla^n\right]\mathcal{F}_n\right\}d\Omega \tag{28}$$

It should be noted that Ψ_k is the k-th moment of the generic even parity flux, not the n-th scalar moment ϕ_n in the SPn equation. Now, one can derive the exact expression of Ψ_k and J_k using $\mathcal{F}_n$.

In the special case of SP3, we have the following terms on the y-z surface:

$$\Psi_0(r) = \frac{1}{4}\phi_0 + \frac{5}{16}\left[\phi_2 - \frac{3}{2}\left(\frac{\partial^2}{\partial y^2}+\frac{\partial^2}{\partial z^2}\right)\left(\frac{2}{15\Sigma_t^2}\phi_0 + \frac{11}{21\Sigma_t^2}\phi_2\right)\right] \tag{29}$$

$$\Psi_2(r) = \frac{1}{16}\phi_0 + \frac{5}{16}\left[\phi_2 - \frac{3}{2}\left(\frac{\partial^2}{\partial y^2}+\frac{\partial^2}{\partial z^2}\right)\left(\frac{2}{15\Sigma_t^2}\phi_0 + \frac{11}{21\Sigma_t^2}\phi_2\right)\right] \tag{30}$$

$$J_1(r) = -\frac{1}{3\Sigma_t}\frac{\partial}{\partial x}(\phi_0 + 2\phi_2) \tag{31}$$

$$\begin{aligned} J_3(r) = -\frac{9}{35\Sigma_t}\Bigg[&\frac{\partial}{\partial x}\phi_2 - \frac{5}{2}\frac{\partial}{\partial x}\left(\frac{\partial^2}{\partial y^2}+\frac{\partial^2}{\partial z^2}\right)\left(\frac{2}{15\Sigma_t^2}\phi_0 + \frac{11}{21\Sigma_t^2}\phi_2\right) \\ &- \frac{2}{15\Sigma_t}\frac{\partial}{\partial x}(\phi_0 + 2\phi_2)\Bigg] \end{aligned} \tag{32}$$

By comparing with the conventional SP3 theory, the new theory contains additional terms involving the part of the divergence in the tangential directions of the surface. The continuity of Eq. (30) and (32) imply that the following two quantities should be continuous on the node surface:

$$\tilde{\phi}_2 = \phi_2 - \frac{3}{2}\left(\frac{\partial^2}{\partial y^2}+\frac{\partial^2}{\partial z^2}\right)\left(\frac{2}{15\Sigma_t^2}\phi_0 + \frac{11}{21\Sigma_t^2}\phi_2\right) \tag{33}$$

$$\tilde{J}_3 = -\frac{1}{\Sigma_t}\left[\frac{\partial}{\partial x}\phi_2 - \frac{5}{2}\frac{\partial}{\partial x}\left(\frac{\partial^2}{\partial y^2}+\frac{\partial^2}{\partial z^2}\right)\left(\frac{2}{15\Sigma_t^2}\phi_0 + \frac{11}{21\Sigma_t^2}\phi_2\right)\right]. \tag{34}$$

It is worth mentioning that the two terms $\tilde{\phi}_2$ and $\tilde{J}_3$ are different from the usual *ad hoc* continuity conditions for ϕ_2 and J_3, which will no longer be continuous on the surface in the new theory.

3.2. Implementation of interface and boundary conditions

Converting the tangential divergence to the normal component of the divergence by applying the relationship $\frac{\partial^2}{\partial y^2}+\frac{\partial^2}{\partial z^2} = \nabla^2 - \frac{\partial^2}{\partial x^2}$ to Eq. (33) and (34), we arrive at the interface and boundary conditions for the SP$_3$ theory:

$$\tilde{\phi}_2 = \phi_2 - \frac{3}{2}\delta \tag{35}$$

$$\tilde{J}_3 = -\frac{9}{35\Sigma_t}\frac{\partial}{\partial x}\left(\phi_2 - \frac{5}{2}\delta\right) + \frac{2}{5}J_1, \tag{36}$$

where

$$\delta = \phi_2 - \frac{\partial^2}{\partial x^2}\left(\frac{2}{15\Sigma_t\Sigma_{r,1}}\phi_0 + \frac{11}{21\Sigma_t^2}\phi_2\right). \tag{37}$$

Again, the δ term above is a transport correction to the traditional *ad hoc* conditions and it represents the effect of the transverse terms.

Using Eq. (26) and the definition of transport corrected terms in Eq. (33) and (34), Eq. (29) and (30) becomes:

$$\Psi_0(r) = \frac{1}{2}(j_1^+ + j_1^-) = \frac{1}{4}\phi_0 + \frac{5}{16}\tilde{\phi}_2 \tag{38}$$

$$\Psi_2(r) = \frac{1}{2}(j_3^+ + j_3^-) = \frac{1}{16}\phi_0 + \frac{5}{16}\tilde{\phi}_2 \tag{39}$$

Note that $\tilde{J}_3 = \tilde{j}_3^+ - \tilde{j}_3^-$ and the corrected partial currents $\tilde{j}_3^+$ and $\tilde{j}_3^-$ are different from the previously defined j_3^+ and j_3^-. Rearranging the above equations yields the interface and boundary conditions expressed by the partial currents required by the response matrix:

$$\begin{aligned} \phi_0 &= \frac{8}{3}(j_1^+ + j_1^-) - \frac{8}{3}(\tilde{j}_3^+ + \tilde{j}_3^-) \\ \tilde{\phi}_2 &= -\frac{8}{15}(j_1^+ + j_1^-) + \frac{32}{15}(\tilde{j}_3^+ + \tilde{j}_3^-), \end{aligned} \tag{40}$$

Since the nodal expansion in the base SP$_3$ equations is not impacted during the derivation in Section 3.1 and thus still valid for the new SP$_3$ theory, the corrected second moment flux term and third moment net partial current become:

$$\begin{aligned} \tilde{\phi}_2 = \phi_2 - \frac{3}{2}\Bigg\{ & \phi_2 - \frac{2}{15\Sigma_t\Sigma_{r,1}}\left[\frac{6}{\Delta x^2}a_2 + \frac{6x}{\Delta x^3}a_3 + \left(\frac{12x^2}{\Delta x^4} - \frac{3}{5\Delta x^2}\right)a_4\right] \\ & - \frac{9}{35\Sigma_t^2}\left[\frac{6}{\Delta x^2}b_2 + \frac{6x}{\Delta x^3}b_3 + \left(\frac{12x^2}{\Delta x^4} - \frac{3}{5\Delta x^2}\right)b_4\right]\Bigg\} \end{aligned} \tag{41}$$

$$\begin{aligned} \tilde{J}_3 = & -\frac{9}{35\Sigma_t}\left[\frac{1}{\Delta x}b_1 + \frac{6}{\Delta x^2}b_2 + \left(\frac{3x^2}{\Delta x^3} - \frac{1}{4\Delta x}\right)b_3 + \left(\frac{4x^3}{\Delta x^4} - \frac{3}{5\Delta x^2}\right)b_4\right] \\ & + \frac{5}{2\Sigma_t}\left(\frac{6}{\Delta x^3}a_3 + \frac{24x}{\Delta x^4}a_4 + \frac{6}{\Delta x^3}b_3 + \frac{24x}{\Delta x^4}b_4\right) + \frac{2}{5}J_1. \end{aligned} \tag{42}$$

Take the right node surface in the x-direction for example, the corresponding node interface flux and net current terms as appeared in Eq. (13) and (14) can be derived as the following:

$$\begin{aligned} \phi_{2,R} = \tilde{\phi}_{2,R} - \frac{3}{2}\Bigg\{ & \phi_{2,R} - \frac{2}{15\Sigma_t\Sigma_{r,1}}\left[\frac{6}{\Delta x^2}a_2 + \frac{6x}{\Delta x^3}a_3 + \left(\frac{12x^2}{\Delta x^4} - \frac{3}{5\Delta x^2}\right)a_4\right] \\ & - \frac{9}{35\Sigma_t^2}\left[\frac{6}{\Delta x^2}b_2 + \frac{6x}{\Delta x^3}b_3 + \left(\frac{12x^2}{\Delta x^4} - \frac{3}{5\Delta x^2}\right)b_4\right]\Bigg\} \end{aligned} \tag{43}$$

$$\begin{aligned} \tilde{j}_{3,R}^+ - \tilde{j}_{3,R}^- = & -\frac{9}{35\Sigma_t}\left[\frac{1}{\Delta x}b_1 + \frac{6}{\Delta x^2}b_2 + \left(\frac{3x^2}{\Delta x^3} - \frac{1}{4\Delta x}\right)b_3 + \left(\frac{4x^3}{\Delta x^4} - \frac{3}{5\Delta x^2}\right)b_4\right] \\ & + \frac{5}{2\Sigma_t}\left(\frac{6}{\Delta x^3}a_3 + \frac{24x}{\Delta x^4}a_4 + \frac{6}{\Delta x^3}b_3 + \frac{24x}{\Delta x^4}b_4\right) + \frac{2}{5}(j_{1,R}^+ - j_{1,R}^-) \end{aligned} \tag{44}$$

Follow the same procedure described in Section 2, a set of equations like the original response matrix based on the partial currents on the node surface can be derived. We can use the same inner/outer iteration scheme to solve the response matrix and the corrected terms $\tilde{\phi}_2$ and $\tilde{J}_3$ will be obtained in addition to Φ_0 and J_1.

4. Equivalent Calculation Scheme

As shown previously, the nodal SP$_3$ solver performs the finite volume integration, which requires material parameters being constant in the node. Fuel pin homogenized cross sections are prepared using the flux-volume weighting procedure to preserve reaction rates between lattice calculations and SP$_3$ calculations. Here, we will only focus on the DF generation approach developed and implemented for the SP$_3$ solver aiming to preserve the leakage rate between nodes.

4.1. SP$_3$ Discontinuity Factors

The derivation above shows that the DFs needed to be used in homogenized nodes can be generated without ambiguity by using the particular SP_N angular flux solution. The work presented below is similar to a previous effort [16] in the sense that the DFs are generated for both zeroth and second order flux moments; however, angular moments in the SP_3 method are different and thus the application of DFs. It should be emphasized that the DF is defined for and applied to Ψ_0 and Ψ_2 in the following way

$$DF_0 = \frac{\Psi_0^{\text{het}}}{\Psi_0^{\text{hom}}}, DF_2 = \frac{\Psi_2^{\text{het}}}{\Psi_2^{\text{hom}}} \tag{45}$$

instead of Φ_0 and ϕ_0, the unknowns in the SP_3 equations. In other words, given a surface limiting two adjacent homogenized regions, the DFs enforce the continuity for the heterogeneous reconstructed flux $DF_0^- \Psi_0^{\text{hom},-} = DF_0^+ \Psi_0^{\text{hom},+}$ and $DF_2^- \Psi_2^{\text{hom},-} = DF_2^+ \Psi_2^{\text{hom},+}$.

The flux solutions from both heterogeneous and homogeneous models are required to compute DFs. The former can be obtained from transport calculations, while the latter needs to be calculated by imposing the conditions of conserving the total net current from the reference heterogeneous transport calculation. It can be seen in Eq. (29-32) that the reference value of Ψ_0, Ψ_2, J_1, and J_3 can all be readily computed in the transport calculation. The resulting values of J_1 and J_3 will then be imposed on each surface of a node (pin cell) as the boundary condition to uniquely determine the SP_3 solution (Ψ_0^{hom} and Ψ_2^{hom}) inside the homogenized cell.

In the context of response matrix in NEM, the updated incoming currents must be adjusted by the net current obtained in the transport solution, that is, by adding the net current to the outgoing current of the neighboring nodes. This leads to solving a fixed interface problem using the homogenized cross sections while also fixing the eigenvalue, which is like the calculation scheme described in [17]. For this purpose, an independent program DF Generation Routine (DFGR) is developed to generate the homogeneous solutions. It can take the eigenvalue, cell interface net currents, and cell averaged scalar fluxes from the transport calculation and solve the fixed interface problem. Unlike the eigenvalue problem, no interactions between nodes are assumed here and each pin cell can be solved individually.

As depicted in Figure 1, the equivalent calculation process devised for the SP_3 solver can be carried out in the following steps:

1. Perform the transport calculations and generate quantities including k_{eff}, cell homogenized cross sections, cell averaged scalar flux, and side-dependent surface fluxes and currents.
2. Solve the fixed interface problem for each cell sequentially by taking the reference values obtained in Step 1, generate the SP_3 surface fluxes and currents, then compute the DFs according to their definitions.
3. Execute normal SP3 calculation on a pin-by-pin level using the homogenized cross sections from Step 1 and DFs from Step 2 to obtain the SP_3 solution.

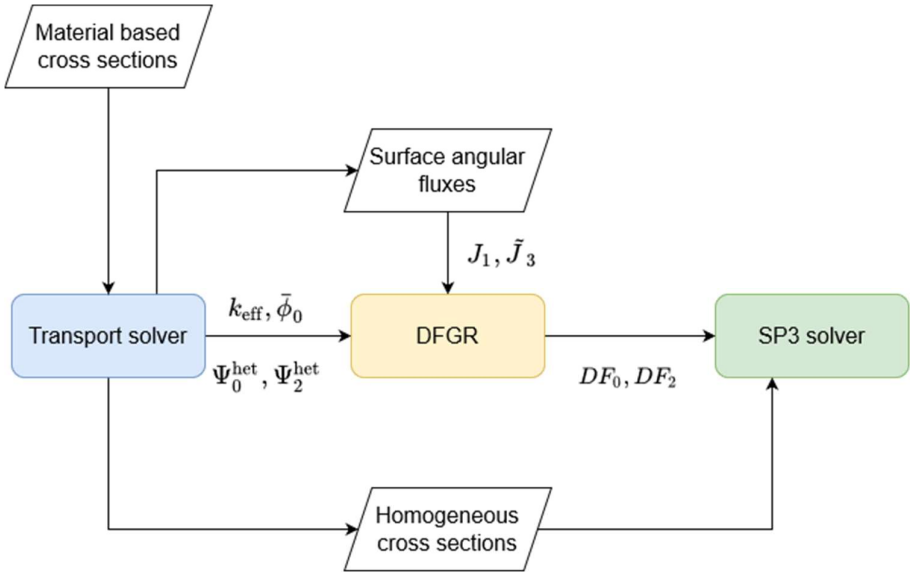

Figure 1. Procedure of equivalent core calculation using SP_3 solver.

4.2. Practical Approach to Generate SP_3 Discontinuity Factors

The equivalent calculation procedure presented above relies on the whole-core transport solutions, which is not practical in routine calculations and, in a way, defeats the purpose of using low order solvers like SP_3. Therefore, efforts are also made to explore the feasibility of color set lattice models to generate equivalent parameters for the core simulation. The three color set models under consideration are:

1. Single-pin model: cross sections are homogenized over the pin cell and DFs are calculated for each of the four surfaces of a pin cell.
2. Double-pin model: two pin cells of different type (i.e., material) are placed next to each other and DFs are calculated for each of the four surfaces in each pin cell. The cross sections are taken from the first model.
3. Assembly model: both homogenized cross sections and DFs are location dependent, i.e., they are generated for each of the pin cells.

The reflective boundary condition is applied to all three models. Among the three models, the first one is the simplest one and does not capture the leakage between different fuel pins and thus is expected to result in the worse performance. The second one capture the effect from neighboring effects to a certain extend but the total number of models increases significantly with the types of fuel pin. The last model supports location dependent pin-wise homogenizations and DF generation in an environment that is like that in the core.

5. Verification of Transported Corrected SP_3 Solver

The newly developed transported corrected SP_3 solver and the corresponding equivalent calculation scheme are verified using the C5G7 benchmark [18]. It is a miniature light water reactor (LWR) with sixteen fuel assemblies (mini core): eight uranium oxide (UO_2) assemblies and eight mixed oxide (MOX) assemblies, surrounded by a water reflector. It features a quarter-core radial symmetry in the 2-D configuration, as shown in Figure 2. On the fuel pin level, there are one UO_2 pin, three MOX pin, one guide tube, and one fission chamber. The three MOX fuels pins are 4.3%, 7.0%, and 8.7% plutonium weight enriched.

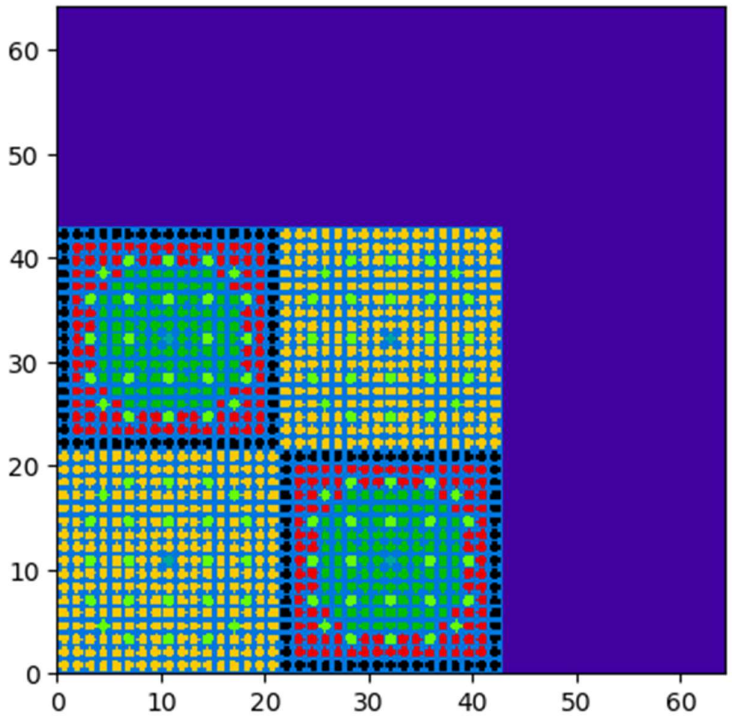

Figure 2. OpenMOC model for C5G7 core. Materials are distinguished by different colors.

In this study, only the core geometry is adopted, and a new set of cross sections is generated in a 7-group energy structure because the original cross sections prepared by the benchmark do not satisfy the unique requirement of SP_3 solver [10].

The transport code OpenMOC [19] is selected to perform the reference transport calculation because of the convenience of the code to extract node interfaces angular fluxes for DFs generations. However, because the current version only accepts isotropic scattering cross sections, transport corrections are applied to modify isotropic scattering cross sections. All the transport calculations shown below are conducted using the long characteristic method with 32 azimuthal angles, 3 polar angles, the ray trace width of 0.03 cm, and the eigenvalue convergence criterion of 1×10^{-7}.

5.1. Transport Corrected SP_3 Method

First, we compare the performance of the base and transport corrected SP_3 solver without applying DFs to reveal the impact of the updated interface and boundary conditions. Three cases are selected from the C5G7 benchmark for this purpose, including the UO_2 assembly, MOX assembly, and C5G7 core. In the single assembly cases, pin-wise cross sections are generated using the assembly model with the infinite lattice approximation. For the last case, they are prepared in whole-core transport calculation, including the cross sections of the water reflector.

The comparison of the eigenvalue yields negligible differences (less than 10 pcm in all cases), which indicates the correction term δ in Eq. (37) is small and thus has a trivial impact on integral parameters like k_{eff}. The focus has been shifted to local quantities. The absolute relative error in the pin power at all locations is first computed for both solvers as $d = |p_{\text{SP3}}/p_{\text{MOC}} - 1|$, where p denotes the normalized pin power. Then, the difference between the two solvers is calculated as $\Delta = d_t - d_b$, where the subscript t means "transport corrected" and b refers to "base". The value of Δ is plotted for the C5G7 core problem according to the pin location, as shown in Figure 3.

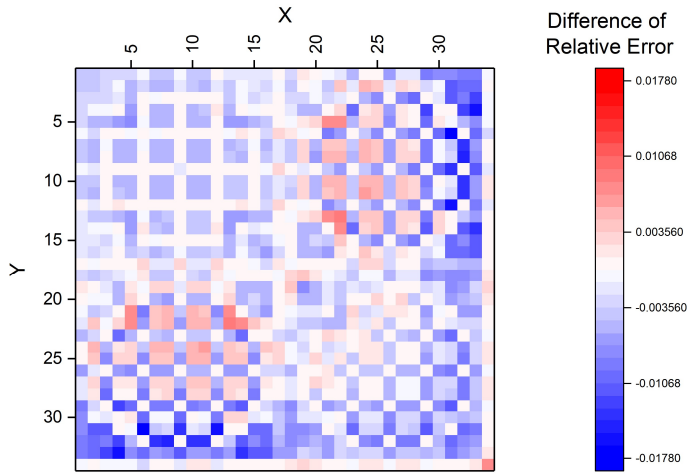

Figure 3. Differences in relative pin power using the base and transport corrected SP_3 solvers. Blue regions indicate improved predictions by the transport corrected SP_3 solver while red regions mean the opposite.

The blue regions in the distribution indicate the improved prediction accuracy due to the correction to the interface and boundary conditions. It can be seen that the transport corrected SP_3 solver yields slightly better pin power distributions, especially at the center of the UO_2 assembly (upper left assembly), regions close to the water reflector (right and bottom surfaces), as well as pin cells next to the fission chamber and guide tubes. As expected, the transport corrected solver cannot eliminate the prediction error because the spatial homogenization errors still exist.

5.2. Test and Comparison of DFs

Next, the performance of DFs is tested and analyzed in full equivalent calculations. In addition to the three cases used in the previous sub-section, a C5 core problem is also introduced. It contains only fuel assemblies with reflective boundary conditions applied to the outer surface of the geometry. This case would help reveal the impact of DFs on the assembly interfaces by eliminating the effects of the reflector. Following the reference transport calculation, the procedure depicted in Figure 1 is carried out to generate equivalent parameters, inducing the pin-wise cross sections and side-dependent DFs. The equivalent parameters are generated for and applied to each case independently.

It is worth mentioning that numerical instability emerges in regions experiencing high flux gradient after applying DFs to the NEM response matrix, which forces the spatial discretization to be further refined to achieve convergence. As a result, each pin cell is subdivided into 4 nodes in equal size and the DFs are only imposed on the outer surface of the pin cell. The refinement allows the flux gradient to occur inside the pin cell; however, the flux is assumed to be constant across surfaces within each pin cell when the DFs are generated. This inconsistency will inevitably introduce errors to the SP_3 calculation.

Table 2 compares the performance of the transport corrected SP_3 solver in terms of its prediction of eigenvalue and pin power distribution. It can be seen that DFs of the GET help reduce the prediction error significantly in all four test cases. The largest improvement is observed in the C5G7 core case, where the deviation from the reference value is reduced by ~200 pcm in eigenvalue and over halved in the root-mean-square (RMS) error of pin power distribution. The prediction accuracy is also drastically improved in the MOX assembly case where the local flux gradient is more profound than that in the UO_2 assembly.

In principle, if the equivalent calculation is conducted properly, the low order operator should reproduce the transport solutions. The non-zero deviations from the reference solution as shown in Table 1 indicate that the inconsistency between the DF generation and application introduced by the refined 2×2 meshing prevent the full equivalent

calculation from being performed. Another source of deviation in the last test case stems from the fact that DFs for the nodes in the water reflector are all assumed to be 1 due to the limitation of the DFGR program. It would tilde the flux distribution in regions across the core/reflector boundary.

Table 1. Performance of the transport corrected NEM SP_3 solver on various benchmark problems. The deviation from the reference results is given in pcm for the eigenvalue and RMS error for the pin power distribution.

Test case	Solver	Δk_{eff} (pcm)	RMS error of pin power
UO_2 assembly	NEM SP_3	-125	0.010
	NEM SP_3 w/ DFs	-5	0.004
MOX assembly	NEM SP_3	-38	0.008
	NEM SP_3 w/ DFs	10	0.001
C5 core	NEM SP_3	-171	0.048
	NEM SP_3 w/ DFs	-75	0.023
C5G7 core	NEM SP_3	269	0.049
	NEM SP_3 w/ DFs	-59	0.023

Next, various color set models are tested for their capability to facilitate practical equivalent calculations, because generating equivalent parameters from the whole-core transport solution defeats the purpose of homogenization. The three color set models described previously are:

1. Single-pin model: There are 7 models each corresponding to one type of pins. The non-fissionable node, such as guide tubes and water reflector cells, is placed in the center of a 3×3 configuration surrounded by UO_2 fuel pins.
2. Double-pin model: Eight sets of 2×1 pin color set models are developed for different combination of pin cells. These DFs will be used in the whole core on the interface between neighboring different cells.
3. Assembly model: Single UO_2 and MOX assembly models.

A fourth model is also considered which is a mix of Option 2 and 3. The DFs from the assembly color set are used on node interfaces inside an assembly, while those from the double-pin color set are used on the assembly interfaces. The comparison of the results of the C5G7 core calculation is listed in Table 2.

Table 2. Performance of the transport corrected SP_3 solver using different DF generation models. The deviation from the reference results is given in pcm for the eigenvalue and RMS error for the pin power distribution.

Colorset model	Δk_{eff} (pcm)	RMS error of pin power
Single-pin	273	0.056
Double-pin	336	0.056
Assembly	288	0.048
Assembly + double-pin	272	0.047

We observe that the calculation accuracy in terms of the eigenvalue and pin power distribution is improved slightly and consistently as the size of the color set model increases. The assembly model shows better results than the single-pin and double-pin models and the addition of DFs on the assembly interfaces from the double-pin model (Option 4) further reduces the prediction error. This result indicates that the mixed DFs manage to find a good compromise between local and global trends.

However, it is somewhat out of expectation that none of the color set models significantly outperform the approach without DFs in Table 1. That is to use only the location-dependent cross sections generated from the whole-core reference transport solution, although the associated computational cost in the latter case would be massively elevated. The results seem to imply that the impact of two factors in the equivalent calculation, the homogenized cross sections, and DFs, almost contribute equally to the prediction

accuracy. Effort will be made in the future to determine the optimal approach to perform equivalent calculation for the SP_3 solver.

6. Conclusions and Outlook

In this work, we focus on the development of a transport corrected nodal SP_3 solver for the equivalent reactor core calculation. The response matrix in NEM SP_3 solver has been reformulated based on the recent published new SP_3 theory with rigorously derived interface and boundary conditions, while the computation scheme in NEM is kept intact. A streamlined process of generating DFs of the GET for the correction of homogenization error has been implemented, which incorporates the high-fidelity transport code and an in-house developed DF generation program. We also propose a few models with varying sizes for the generation of equivalent parameters aiming to further reduce the computational burden and explore their feasibility to practical applications. The transport corrected SP_3 solver and various color set models are tested on the mini-core C5G7 benchmark problem.

It was found that the transport corrected SP_3 solver can compute the inter-node leakage rate correctly due to the updated interface and boundary conditions and thus improve the prediction of the pin power distribution. In the whole-core calculation, the regions benefiting the largest improvement are located at the center of the core, close to the water reflector, and next to the fission chamber and guide tubes.

The performance of DFs is tested and analyzed in full equivalent calculations. We can see that DFs of the GET help reduce the prediction error significantly in all test cases from the single assembly, active core, and core with reflectors. In the last case, the deviation from the reference transport solutions is reduced by ~200 pcm in eigenvalue and over halved in the RMS error of pin power distribution. In order to increase the feasibility of the equivalent calculation scheme to practical applications, a number of color set models are introduced and analyzed, including the single-pin, double-pin and assembly models. It is shown that the mixed DFs option outperforms all other configurations in terms of eigenvalue and power distribution predictions, indicating that this option can reach a satisfying compromise between local and global trends. With DFs, the assembly color set model slightly outperforms the most accurate homogenization approach without DFs while maintaining a superior computational efficiency.

This study has also identified a few discrepancies in the implementation of the transport corrected SP_3 methodology. For example, it has experienced numerical instabilities which cause issue to achieve converged solution when the DFs are imposed. Our preliminary investigation points it to the use of the 1-D forth order polynomial nodal expansion method implemented in the NEM solution method. We plan to implement and test a semi-analytical nodal expansion method in the future work to resolve this issue.

The inability to generate DFs for the water nodes in the reflectors is also found to be partially responsible to the deviations of the SP_3 results from the reference transport solution. Thus, the DF generation program will be revisited and updated to solve the fixed interface problem for the reflector region. At last, effort will continue to investigate color set models that can maximize the benefit of the equivalent calculations while maintaining the computational cost to a reasonable level for practical whole-core simulations.

Author Contributions: Conceptualization, J.H. and K.I..; methodology, Y.X., J.H., K.I.; formal analysis, Y.X. and J.H.; investigation, Y.X.; resources, J.H. and K.I.; data curation, Y.X.; writing—original draft preparation, Y.X. and J.H.; writing—review and editing, J.H. and K.I.; visualization, Y.X.; supervision, J.H. and K.I.; project administration, J.H. and K.I.; funding acquisition, J.H. and K.I. All authors have read and agreed to the published version of the manuscript.

Funding: This research received no external funding.

Conflicts of Interest: The authors declare no conflict of interest.

References

1. Gelbard, E. M. Application of spherical harmonics method to reactor problems. Bettis Atomic Power Laboratory, West Mifflin, PA, Technical Report No. WAPD-BT-20, 1960.
2. Pomraning, G. Asymptotic and variational derivations of the simplified P_N equations. *Annals of Nuclear Energy* **1993**, *20(9)*, 623–637.
3. Larsen, E. W.; Morel, J. E.; McGhee, J. M. Asymptotic Derivation of the Multigroup P_1 and Simplified P_N Equations with Anisotropic Scattering. *Nuclear Science and Engineering* **1996**, 123, 328-342.
4. Brantley, P. S.; Larsen, E.W. The simplified P3 approximation. *Nuclear Science and Engineering* **2000**, *134.1*, 1–21.
5. Litskevich, D.; Merk, B. SP3 solution versus diffusion solution in pin-by-pin calculations and conclusions concerning advanced methods. *Journal of Computational and Theoretical Transport* **2014**, 43 (1-7), 214-239.
6. Kozlowski, T.; Xu, Y.; Downar, T. J.; Lee, D. Cell homogenization method for pin-by-pin neutron transport calculations, *Nuclear Science and Engineering* **2011** 169 (1), 1-18.
7. Yu, L.; Lu, D.; Chao, Y. A. The calculation method for SP_3 discontinuity factor and its application. *Annals of Nuclear Energy* **2014**, 69: 14-24.
8. Thompson, S. A., Ivanov. K. N. Advances in the Pennsylvania State University NEM code. *Annals of Nuclear Energy* **2016**, *94*, 251-262.
9. Xu, Y.; Hou, J.; Ivanov, K. Improvement to NEM SP_3 Modelling and Simulation. In: Proceedings of PHYSOR 2020, Cambridge, United Kingdom, March 29-April 2, 2020.
10. Xu, Y.; Hou, J.; Ivanov, K. Implementation of Second-Order Discontinuity Factor for Simplified P3 Theory in NEM. In: Proceedings of PHYSOR 2018: Reactors Physics paving the way towards more efficient systems, Cancun, Mexico, April 22-26, 2018.
11. Chao, Y. A. A new and rigorous SP_N theory for piecewise homogeneous regions. *Annals of Nuclear Energy* **2016**, *96*, 112–125.
12. Chao, Y. A. A new and rigorous SPN theory–Part II: Generalization to GSPN. *Annals of Nuclear Energy* **2017**, 110, 1176–1196.
13. Xu, Y. Generalized equivalent nodal SP_3 methodology for reactor simulations. Doctoral dissertation, North Carolina State University, Raleigh, NC, 2020.
14. Smith, K. Assembly homogenization techniques for light water reactor analysis. *Progress in Nuclear Energy* **1986**, 17, 3, 303 – 335.
15. Koebke, K. A new approach to homogenization and group condensation. No. IAEA-TECDOC-231. 1980.
16. Yamamoto, A.; Sakamoto, T.; Endo, T. Discontinuity factors for simplified P_3 theory. *Nuclear Science and Engineering* **2016**, *183*.1, 39–51.
17. Chao, Y. A.; Yamamoto, A. The explicit representation for the angular flux solution in the simplified P_N (SP_N) theory. In Proceedings of PHYSOR 2012: Advances in Reactor Physics Linking Research, Industry, and Education, Knoxville, Tennessee, April 2012.
18. Lewis, E. E., et al. Benchmark specification for Deterministic 2-D/3-D MOX fuel assembly transport calculations without spatial homogenization (C5G7 MOX). NEA/NSC 280, 2001.
19. Boyd, W. et al. The OpenMOC Method of Characteristics Neutral Particle Transport Code. *Annals of Nuclear Energy* **2014**, 68, 43–52.